Separation Science and Technology
Publication details, including instructions for authors and subscription information:
http://www.informaworld.com/smpp/title~content=t713708471

Separation of Methane and Nitrogen by Adsorption on Carbon Molecular Sieve

Simone Cavenati[a]; Carlos A. Grande[a]; Alírio E. Rodrigues[a]
[a] Laboratory of Separation and Reaction Engineering (LSRE), Department of Chemical Engineering, Faculty of Engineering, University of Porto, Porto, Portugal

To cite this Article Cavenati, Simone , Grande, Carlos A. and Rodrigues, Alírio E.(2005) 'Separation of Methane and Nitrogen by Adsorption on Carbon Molecular Sieve', Separation Science and Technology, 40: 13, 2721 — 2743
To link to this Article: DOI: 10.1080/01496390500287846
URL: http://dx.doi.org/10.1080/01496390500287846

Separation Science and Technology, 40: 2721–2743, 2005

ISSN 0149-6395 print/1520-5754 online
DOI: 10.1080/01496390500287846

Separation of Methane and Nitrogen by Adsorption on Carbon Molecular Sieve

Simone Cavenati, Carlos A. Grande, and Alírio E. Rodrigues
Laboratory of Separation and Reaction Engineering (LSRE), Department of Chemical Engineering, Faculty of Engineering, University of Porto, Porto, Portugal

Abstract: Adsorption equilibrium of methane and nitrogen on CMS 3K from Takeda Corp. were gravimetrically measured at 298, 308, and 323 K and at pressures up to 2000 kPa. The most adsorbed gas is methane followed by nitrogen. The adsorption loading at 550 kPa and 308 K is 1.73 mol/kg for methane and 0.91 mol/kg for nitrogen. Experimental data were fitted with the multisite Langmuir model. Single component uptake of these gases at low pressures was used to determine the adsorption kinetics. Adsorption of nitrogen is much faster than methane, although this gas is preferentially adsorbed. The adsorption rate of both gases was controlled by a surface barrier resistance at the mouth of the micropore combined with micropore diffusion. Breakthrough curves of pure gases and their binary mixtures were measured at ambient temperature. A bi-LDF (Linear Driving Force) model was used to predict the fixed-bed behavior. Large differences in the adsorption kinetics were observed: at 308 K the LDF constant ratio was $K_{\mu,N_2}/K_{\mu,CH_4} = 133$, although because of much higher adsorption of methane, the overall kinetic selectivity was 1.9 at 308 K. The data obtained in this work can be used for adsorption separation processes modeling for methane purification from nitrogen-contaminated streams.

Keywords: Carbon molecular sieve, adsorption properties, methane, nitrogen, binary adsorption

Received 9 December 2004, Accepted 21 July 2005

Address correspondence to Alírio E. Rodrigues, Laboratory of Separation and Reaction Engineering (LSRE), Department of Chemical Engineering, Faculty of Engineering, University of Porto, Rua Dr. Roberto Frias s/n, 4200-465, Porto, Portugal. Fax: +351 22 508 1674; E-mail: arodrig@fe.up.pt

INTRODUCTION

The main application of a separation technology involving methane and nitrogen is in the natural gas (NG) field. NG refers to the gaseous fossil-based fluid found in geological accumulations widespread all over the world. Natural gas is a valuable alternative fuel and has two advantages in comparison with other combustibles: it is clean-burning and has a lower cost, being cheaper than other fuels like crude oil, gasoline, or diesel, for example. In the environmental protection field by using NG as a vehicular fuel reductions in CO, CO_2, and SO_2 are 97, 24, and 90%, respectively, and the amount of lead discharged in exhaust gases is reduced to zero. Currently, NG supplies one-fourth of the energy needed in the world's homes, businesses, vehicles, industries, and power plants, and the consumption of NG is expected to grow by 50% over the next 20 years (1).

The composition of natural gas varies considerably according to the location of the drill; it consists mainly of methane, typically 80–95%, with variable amounts of C_{2+} hydrocarbons, and often nitrogen and carbon dioxide as impurities (2). Nitrogen is a major problem in many fields; i.e., 16% of U.S. reserves are contaminated with higher amounts of nitrogen than required by pipeline specifications.

Natural gas from a field will burn without processing, but it usually requires treatment to remove and control the level of particular components affecting regulatory compliance of product quality and also for transportation in pipelines. To meet "pipeline quality methane" the maximum amount of nitrogen and carbon dioxide cannot exceed 4 and 2%, respectively. The carbon dioxide reduction is also important to prevent equipment and pipeline corrosion.

Methane–nitrogen separation can also appear in methane upgrading from landfill gas (LFG) production (3). When the LFG is collected above atmospheric pressure, a low amount of nitrogen and oxygen is found in a stream mainly composed of methane and carbon dioxide (4). To increase methane yield, methane may be collected at pressures below atmospheric allowing more air to penetrate the cap and releasing more nitrogen into the product stream (oxygen is consumed aerobically). To produce pipeline methane a series of PSA units in series was proposed to split CO_2 followed by N_2, being this nitrogen rejection process the most expensive in the process economics (3). A similar perspective in economic limitations was reported for gob and coalbed methane enrichment (5).

Nitrogen-contaminated NG and LFG streams have a low BTU value and have to be upgraded by nitrogen removal. Some fields cannot be exploited because of the economical constraints of nitrogen removal (traditionally by techniques such as cryogenic distillation) and most of the exploited ones are supported by the extraction of helium as a byproduct.

Separation of gas mixtures by pressure swing adsorption (PSA) has emerged as a very successful technology and has gained wide commercial

acceptance in the last years. It is generally accepted that methane-nitrogen is a very difficult separation due to the low selectivity of the adsorbents. A fundamental requirement of an adsorbent for this separation is to exhibit nonadsorbing characteristics toward methane. Even when many commercial adsorbents were tested for this separation, most of them (particularly zeolites and activated carbons) adsorb more methane than nitrogen (6–9). A process using one of these adsorbents will deliver the product (purified methane) at low pressure requiring an additional compression stage. A new group of tailored titanosilicate (named ETS, Engelhard titanosilicates) molecular sieves is promising (10) because of the possibility of total exclusion of the methane molecule. Particularly, a PSA process using modified-ETS-4 (named Molecular Gate®) is being commercialized since 2001 splitting a stream of methane with 18% of nitrogen (11).

Carbon molecular sieves (CMS) are carbonaceous adsorbents with a relatively narrow micropore size distribution that can be produced from many different organic sources: bituminous coal, bones, coconut shell, etc. The final micropore size depends on the pyrolysis and activation steps in the manufacturing process (12). Carbon molecular sieves are known to offer significant kinetic selectivity between compounds of similar sizes and properties, like oxygen-nitrogen separation (13–15). Another application where CMS is being applied is the separation of methane and carbon dioxide for landfill gas purification (16, 17). It is also used in carbon dioxide recovery from steel converter gas (18). The molecule of nitrogen has a kinetic diameter of 3.6 Å while the diameter of the molecule of methane is 3.8 Å. Although the difference is small, the pores of a carbon molecular sieve can be bottlenecked to an intermediate size to inhibit or delay the adsorption of methane.

In this paper we will present adsorption equilibrium and kinetics of methane and nitrogen in carbon molecular sieve 3 K from Takeda Corp. at 298, 308, and 323 K. Adsorption equilibrium up to pressures of 2000 kPa is reported for methane and nitrogen. Adsorption kinetics of both gases was determined with uptake curves. Pure gas and binary breakthrough curves were also measured to confirm adsorption equilibrium and kinetics and to provide required data to model a PSA unit for kinetic separation of methane-nitrogen.

EXPERIMENTAL SECTION

Adsorption equilibrium of pure gases was performed in a magnetic suspension microbalance (Rubotherm, Germany) operated in closed system. The sample of adsorbent is weighed and placed in a basket suspended by a permanent magnet through an electromagnet (magnetic suspension coupling). The cell in which the basket is housed is then closed and vacuum is applied. An analytical balance is connected to the magnetic coupling receiving the weight values measured inside the cell and through an acquisition system the data are recorded in a computer. Two Lucas Schaevitz pressure transducers

were used; one from 0–100 kPa and other from 0–25000 kPa to acquire data at low and high pressures, respectively. Adsorption equilibrium was established after some time without significant variation of the weight and pressure: for the case of nitrogen this period was 30 min while for methane (very low diffusing gas) 6 h were established (each point takes around 3 days to achieve equilibrium).

The activation of the sample was carried out under vacuum at 523 K overnight. The heating rate to reach this temperature was 1 K/min. Isotherms were measured at 298, 308, and 323 K. Adsorption and desorption measurements were performed and all the isotherms were reversible.

When the initial point of equilibrium is to be measured, an initial pressure lower than 10 kPa was always established and the adsorption uptake was recorded each 15 s for nitrogen and each 2 min for methane. This initial adsorption uptake of the pure gases at the different temperatures was used for kinetic measurements.

Pure gas and binary breakthrough curves were measured in a laboratorial unit already existing in our laboratory used for C_3 separation (19). To study the adsorption of this mixture, the analysis system (performed by a gas chromatograph, GC) was modified. Pure gas analysis and binary mixtures were performed using a thermal conductivity detector for methane + nitrogen detection and a flame ionization detector for methane measurements. It was assumed (and verified in the calibration) that nitrogen does not produce variations in the FID signal for methane detection. The column used in the GC was a CP-Poraplot Q (Varian, Netherlands) with a flow rate of 7.0 mL/min of helium (used as carrier gas and as TCD reference gas) at constant temperature of 373 K.

The characteristics of this unit are reported in Table 1. In all the cases the column was previously filled with helium. For the pure gas adsorption breakthrough curves, helium was used to establish the molar fraction of the measured gas in the desired value. No inert was introduced in the binary breakthrough experiments. The adsorbent was activated at 523 K overnight under a small flow of helium.

Takeda Corp (Tokyo, Japan) kindly provided the CMS Takeda 3 K extrudates used in this study. Some characteristic properties of the adsorbent are summarized in Table 2. All gases used in this work were provided by Air Liquide: methane N35, nitrogen N45 and helium N50 (purities greater than 99.95, 99.995, and 99.999%, respectively).

THEORETICAL

Adsorption Equilibrium

As a first step in the description of the adsorption equilibrium, we must distinguish between absolute adsorption and excess adsorption. The relation

Table 1. Fixed-bed parameters and adsorbent properties used in binary bed experiments of methane-nitrogen adsorption and in pure fixed-bed experiments of methane-helium and nitrogen-helium adsorption in CMS3K (Takeda)

Bed radius, m	0.0105
Bed length, m	0.83
Bed porosity	0.33
Bulk density, kg/m^3	715.43
Column wall density, kg/m^3	8238
Wall specific heat, J/kg K	500
Wall heat transfer coefficient, W/m^2 K	80.0
Overall heat transfer coefficient, W/m^2 K	25.0
Pellet radius (infinite cylinder), m	0.9E−3
Pellet density, kg/m^3	1060
Pellet porosity	0.46
Total flow rate, SLPM	0.7
Solid specific heat, J/kg K	880
Methane–nitrogen ratios in binary breakthrough experiments	0.43–0.57; 0.57–0.43
Methane molar fractions in pure breakthrough experiments	0.09, 0.43, 0.56, 0.75
Nitrogen molar fractions in pure breakthrough experiments	0.43, 0.53, 0.60, 0.80

between them is shown in Equation (1) (20),

$$q = q_{exc} + \frac{\rho_G V_{ads}}{m_s M_W} \tag{1}$$

where q is absolute adsorbed phase concentration, q_{exc} is excess adsorbed phase concentration, ρ_G is the density of the gas phase, V_{ads} is the volume of the adsorbed phase, m_s is the mass of adsorbent connected to the microbalance, and M_W is the molecular weight of gas. The second term in the right-hand side corresponds to the "buoyancy" correction term. The main

Table 2. Adsorbent properties

Parameters	Value
Pellet density (g/cm^3)	1.06
Extrudate diameter (cm)	0.18
Average extrudate length (cm)	0.43
Pellet porosity (–)	0.46
Macropore radius (Å)	1560
Macropore volume (cm^3/g)	0.313

reason to this difference is that the volume of the adsorbed phase is not negligible, and the gas density becomes closer to the density of the adsorbed phase especially at higher pressures, where the last term of the right-hand side of Eq. (1) cannot be neglected (21). The excess adsorption is obtained from adsorption measurements. On the other hand, the absolute adsorption cannot be obtained directly, and many approximate methods to calculate it from the excess adsorption were published (20–23).

For any measurement in the Rubotherm microbalance, the weight recorded in the microbalance display Δm (taking the first value as reference because we tare the balance at the beginning of the measurements) is expressed by

$$\Delta m - \Delta ZP = m_{ads} - \rho_G(V_{ads} + V_s + V_c) \tag{2}$$

where ΔZP is the variation of the Zero Point value, m_{ads} is the total mass adsorbed, V_s is the volume of the solid adsorbent, and V_c is the volume of the cell where the adsorbent is loaded.

In order to determine the volumes that contribute to the buoyancy effect, a calibration with helium was performed, under the assumption that this gas is not adsorbed ($m_{ads} = V_{ads} = 0$). From this calibration with helium we get

$$\Delta m = \Delta ZP - \frac{M_w}{R_g T}(V_s + V_c)P \tag{3}$$

From the slope of Eq. (3), the volume of the cell (V_c) and the volume of the solid adsorbent (V_s) can be determined, while the intercept corresponds to the buoyancy of the permanent magnet.

To estimate the volume of the adsorbed phase, in this work we used an assumption reported by Dreisbach and coworkers (22), already tested for adsorption equilibrium measurements with these gases up to 5000 kPa on zeolite 13X (24). The assumption is that the volume of the adsorbed phase is approximated by

$$V_{ads} \cong \frac{m_{ads}}{\rho_L} \tag{4}$$

where ρ_L is the density of the adsorbed phase, which is assumed to be equal to the density at the boiling point at 1 atm., selected as the reference state conditions.

Another consideration according to the definitions given is that

$$q = \frac{m_{ads}}{m_s M_W} \tag{5}$$

Rearranging Eq. (2) by taking into account Eq. (4), we obtain

$$q = \frac{\Delta m - \Delta ZP + \rho_G(V_s + V_c)}{m_s M_W} \frac{\rho_L}{\rho_L - \rho_G} \tag{6}$$

In Eq. (6) it can be observed that when the density of the gas is small (compared with the density of the adsorbed phase), the buoyancy correction can be omitted.

Adsorption equilibrium of pure components was fitted using the multisite Langmuir model (25)

$$\frac{q_i^*}{q_{\max,i}} = K_i P\left(1 - \sum \frac{q_i^*}{q_{\max,i}}\right)^{a_i} \tag{7}$$

where q_{max} is the maximum amount adsorbed, a_i is the number of sites occupied per molecule and with an exponential temperature dependence for the adsorption constant K_i described as

$$K_i = K_i^0 \exp\left(\frac{-\Delta H_i}{RT_s}\right) \tag{8}$$

where K_i^0 is the adsorption constant at infinite temperature and $-\Delta H_i$ is the isosteric heat of adsorption, both for component i.

Adsorption Kinetics by Adsorption Uptake

CMS is known to have bidisperse pore structure with macropores from 100–1000 nm and micropores smaller than 1 nm (18). Because of this large size difference, in most of the literature concerning the use of CMS for gas separation, the controlling transport resistance is in the micropores (26).

According to the preparation of the material, the constriction of the pores can be in the micropore mouth or distributed inside it. Both materials will present micropore resistance, although when the restriction is limited only to the pore mouth, a surface barrier resistance may be present (14). Successful description of diffusion in pores with mouth restriction was achieved by adding a barrier mass transfer coefficient to the micropore model (26, 27) and also using a lumped model (26, 28). It has to be pointed out that both models require experimental data for constant determination: LDF constant in the lumped model and barrier mass-transfer coefficient in the distributed model.

In this work we have used a distributed dual-resistance model (barrier mass-transfer and micropore resistances) to determine kinetic parameters from adsorption uptakes performed at low partial pressure of sorbate. Using a low partial pressure we are diminishing the effects of adsorption equilibrium nonlinearity. Also, as the measurements were performed with CMS extrudates, macropore resistance was also considered and as the fluid is stagnant an external mass-transfer resistance was included in the model.

In any gravimetric batch experiment, when the adsorbent is clean, the molar balance for an ideal gas between times 0 and t is (29)

$$C_B(t) = \left[C_{B0} - \frac{m_S}{V_c} - \langle \bar{q} \rangle \right] \tag{9}$$

where C_{B0} and $C_B(t)$ are the initial and bulk gas concentration at time t, V_c is the entire closed microbalance cell volume, R_g is the ideal gas constant and m_s is the adsorbent mass used. The extrudate-averaged adsorbed phase concentration $\langle \bar{q} \rangle$ for an infinite cylinder is defined by

$$\langle \overline{q} \rangle = \frac{2}{\mathrm{R_p^2}} \int_0^{\mathrm{R_p}} \overline{q} \mathrm{R} \ \mathrm{dR} \tag{10}$$

where R_p is the radius of the extrudate and $\overline{q}$ is the microparticle-averaged adsorbed phase concentration. Equation (9) is a mass balance saying that the number of moles initially present in the microbalance cell are finally distributed in the gas phase and adsorbed by the adsorbent.

The mass balance in a volume element of the extrudate is represented by

$$\varepsilon_p \frac{\partial C}{\partial t} + \rho_\mathrm{p} \frac{\partial \overline{\mathrm{q}}}{\partial \mathrm{t}} = \frac{\varepsilon_p D_p}{\mathrm{R}} \frac{\partial}{\partial R} \left(R \frac{\partial C}{\partial R} \right) \tag{11}$$

where ε_p and ρ_p are the porosity and density of the pellet respectively and D_p is the pore diffusivity. The microparticle-averaged adsorbed phase concentration $\overline{q}$ is defined by

$$\overline{q} = \frac{3}{\mathrm{r}_\mu^3} \int_0^{\mathrm{r_c}} q \mathrm{r}^2 \ \mathrm{dr} \tag{12}$$

where r_μ is the radius of the microparticles where micropores are located.

The initial conditions for the extrudate mass balance is

$$C_{(R,0)} = 0 \tag{13}$$

while the boundary conditions are

$$\varepsilon_p D_p \left. \frac{\partial C}{\partial R} \right|_{(t,Rp)} = k_f \left(C_B - C|_{(t,R_P)} \right) \tag{14}$$

$$\left. \frac{\partial C}{\partial R} \right|_{(0,t)} = 0 \tag{15}$$

where k_f is the external mass transfer resistance.

The Fickian description of diffusion in a microparticle is

$$\frac{\partial q}{\partial t} = \frac{1}{r^2} D_\mu \frac{\partial}{\partial r}\left[r^2 \frac{\partial q}{\partial r}\right] \tag{16}$$

where D_μ is the micropore diffusivity. This equation has to be solved with the following initial and boundary conditions

$$q_{(\mathrm{r},0)} = 0 \tag{17}$$

$$\left.\frac{\partial q}{\partial r}\right|_{(0,\mathrm{t})} = 0 \tag{18}$$

$$\frac{3}{\mathrm{r}_\mu} \mathrm{D}_\mu \left.\frac{\partial q}{\partial r}\right|_{r=r_\mu} = k_b (q^* - q)\big|_{\mathrm{r}=\mathrm{r}_\mu} \tag{19}$$

where q^* is the adsorbed phase concentration in equilibrium with $C_{(t,R)}$ and k_b is the barrier mass-transfer coefficient.

The pore diffusivity is a function of the molecular and Knudsen diffusion described by the Bosanquet equation. In this case of pure gas measurements, instead of the molecular diffusivity, the self-diffusivity was employed (30)

$$\frac{1}{D_p} = \frac{\tau_\mathrm{p}}{D_{AA}} + \frac{\tau_\mathrm{p}}{D_K} \tag{20}$$

$$D_{AA} = \frac{4.186.10^{-6}}{M_\mathrm{w}^{1/2}} \frac{P_c^{2/3}}{T_c^{1/6}} \frac{1}{C_B}$$

$$D_K = 9700 \mathrm{r}_\mathrm{p} \sqrt{\frac{T}{M_W}} \tag{21}$$

where τ_p is the tortuosity of the pellet, M_w is the molecular weight of the gas, r_p is the pore radius (cm), and P_c (atm) and T_c (K) are the critical pressure and temperature, respectively. In Eq. (20) the first term of the right-hand side corresponds to the self-diffusivity D_{AA} (cm^2/s) while the other term is the Knudsen diffusion, D_K (cm^2/s). In Eq. (18), bulk gas concentration, C_B has to be expressed in $\mathrm{mol}/\mathrm{cm}^3$.

Fixed-bed Modeling for Multicomponent Breakthrough Curves

When adsorption equilibrium and kinetic properties are determined, the behavior of a mixture of binary mixtures of methane and nitrogen in a fixed-bed can be predicted. For this purpose, the mass, energy, and momentum balances were used. All the equations used for this purpose are detailed in Table 3. This model was already validated for propane and propylene mixtures (19, 31). To simplify the momentum mass balance, the Ergun equation was used to account for pressure drop in the column. This

Table 3. bi-LDF model used for binary breakthrough prediction: (1) Mass balance of component *i*. (2) Ergun equation; (3) Mass transfer to the solid (bi-LDF model); (4) Energy balance in the gas phase; (5) Energy balance in the solid phase; (6) Energy balance on the column wall; (7, 8) LDF constants

1	$$\varepsilon_c \frac{\partial C_i}{\partial t} = \varepsilon_c D_{ax,i} \frac{\partial}{\partial z}\left(C_T \frac{\partial Y_i}{\partial t}\right) - \frac{\partial (uC_i)}{\partial z} - (1-\varepsilon_c)\frac{ak_f}{Bi_i + 1}(C_i - \langle c_i \rangle)$$
2	$$-\frac{\partial P}{\partial z} = -\frac{150\mu(1-\varepsilon_c)^2}{\varepsilon_c^3 d_p^2}u + \frac{1.75(1-\varepsilon_c)\rho}{\varepsilon_c^3 d_p}|u|u$$
3	$$\frac{\partial \langle c_i \rangle}{\partial t} = K_{P,i}\frac{Bi_i}{Bi_i+1}(C_i - \langle c_i \rangle) - \frac{\rho_p}{\varepsilon_p}\frac{\partial \langle \overline{q_i} \rangle}{\partial t}$$
	$$\frac{\partial \langle \overline{q_i} \rangle}{\partial t} = K_{\mu,i}\left(q_i^* - \langle \overline{q_i} \rangle\right)$$
4	$$\varepsilon_c C_T \tilde{C}_v \frac{\partial T_g}{\partial t} = \frac{\partial}{\partial z}\left(\lambda \frac{\partial T_g}{\partial z}\right) - u\ C_T \tilde{C}_p \frac{\partial T_g}{\partial z} + \varepsilon_c R_g T_g \frac{\partial C}{\partial t} - (1-\varepsilon_c)ah_f\left(T_g - T_s\right) - \frac{2\,h_w}{R_w}\left(T_g - T_w\right)$$
5	$$(1-\varepsilon_c)\left[\varepsilon_p \sum_{i=1}^{n} \langle c_i \rangle \tilde{C}_{vi} + \rho_p \sum_{i=1}^{n} \langle \overline{q_i} \rangle \tilde{C}_{v,ads_i} + \rho_p \tilde{C}_{ps}\right]\frac{\partial T_s}{\partial t} = (1-\varepsilon_c)\varepsilon_p R_g T_s \frac{\partial \langle c_i \rangle}{\partial T} + \rho_b \sum_{i=1}^{n}(-\Delta H_i)\frac{\partial \langle \overline{q_i} \rangle}{\partial t} + (1-\varepsilon_c)ah_f\left(T_g - T_s\right)$$
6	$$\rho_w \tilde{C}_{pw}\frac{\partial T_w}{\partial t} = \alpha_w h_w\left(T_g - T_w\right) - \alpha_{wl}U(T_w - T_\infty)$$
7	LDF constant for macropore diffusion: $K_{P,i} = \dfrac{15D_{p,i}}{R_p^2}$
8	LDF constant for micropore resistance: $K_{\mu,i} = \dfrac{1}{1/k_{b,i} + \dfrac{r_\mu^2}{15D_{\mu,i}}}$

equation was also used to consider the velocity as a variable due to bulk adsorption. Also, a linear driving force for macropore and micropore resistances (bi-LDF) was applied instead of the detailed model with macropore, micropore, and surface barrier resistances. Note that the LDF constant for the micropores is calculated using the micropore diffusivity and the surface barrier resistance. The parameters used in the simulations that predict the experimental data are summarized in Table 1, together with the data of the equipment. The bi-LDF model was used instead of the complete model in order to diminish the computational time, simplifying the model to be used in future PSA simulations.

The models used to fit the data of the uptake experiments described by Equations (9)–(21) as well as the model used for prediction of the binary breakthrough curves in a fixed-bed, were numerically solved in gPROMS (PSE Enterprise, UK) using orthogonal collocation of finite elements. Twenty finite elements with two interior collocation points were used in each domain (micropore and macropore) in the uptake model and 40 elements were used in the axial domain in fixed-bed modeling.

ADSORPTION EQUILIBRIUM

Once the helium calibration and buoyancy corrections were performed according to the protocol described in a previous section, the absolute amount adsorbed per gram of adsorbent is obtained as a function of pressure. The adsorption equilibrium isotherms of methane and nitrogen at 298, 308, and 323 K are shown in Figs. 1 and 2, respectively. In these figures, the values obtained directly from the microbalance (corresponding to the excess adsorbed phase) and the absolute adsorbed phase, are shown. The correction was performed according to the explanation given in the previous section. All isotherms were completely reversible. Methane is more adsorbed than nitrogen, particularly at low pressures. Adsorption equilibrium of methane was achieved only after 3 days of gas-adsorbent contact. The isotherms were well fitted with the multisite Langmuir model (solid lines in Figs. 1 and 2). The fitting parameters of the three gases are shown in Table 4. The heat of adsorption also follows the order $CH_4 > N_2$.

Adsorption of these gases in carbon molecular sieves has been extensively reported (4, 8, 16, 17, 32–38). In the different works small differences in the loading of the adsorbents, particularly at low pressures, were observed even for adsorbents from the same manufacturer.

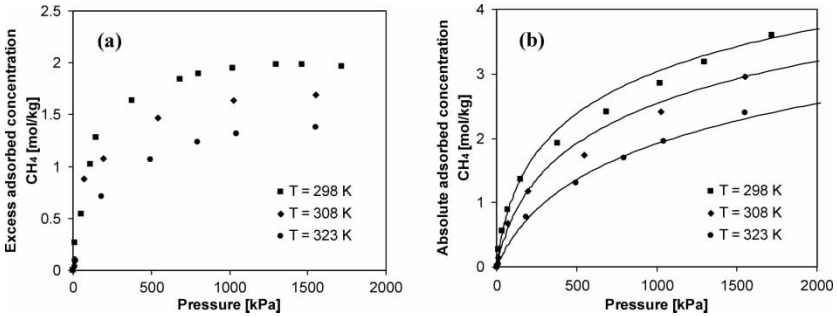

Figure 1. Adsorption equilibrium of methane on Takeda CMS 3K. (a) Excess adsorbed phase concentration determined in the Rubotherm microbalance, (b) absolute adsorbed phase concentration. Symbols: ■ T = 298 K; ◆ T = 308 K; ● T = 323 K; solid lines–multisite Langmuir model.

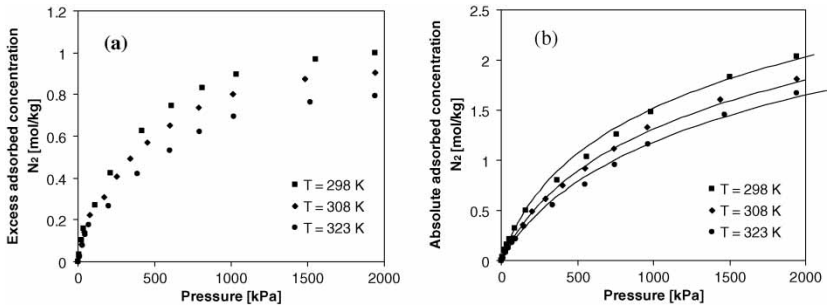

Figure 2. Adsorption equilibrium of nitrogen on Takeda CMS 3K. (a) Excess adsorbed phase concentration determined in the Rubotherm microbalance, (b) absolute adsorbed phase concentration. Symbols: ■ T = 298 K; ◆ T = 308 K; ● T = 323 K; solid lines–multisite Langmuir model.

Adsorption equilibrium of methane on CMS at low temperatures was reported in previous works (4, 8, 16, 38). In the low-pressure range, our work is coincident with the data of Ma et. al. (8), while at pressures up to 500 kPa all works report capacities around 2.25 mol/kg (4, 8, 16, 38). The data also agree with those obtained in CMS membranes in the 0–100 kPa pressure range (32).

Nitrogen adsorption properties are perhaps the most available in literature. In our case, the data in the low and intermediate pressure range (up to 700 kPa) compare well with other published results (8, 13, 33, 34). At pressures higher than 700 kPa our data are in agreement with the work of Bae and coworkers (38) dealing with adsorption equilibrium at high pressures. All the works mentioned here used Takeda CMS while other works with adsorbents from other manufacturer have different loading capacities for these gases even at high pressures (35).

KINETICS OF ADSORPTION BY BATCH UPTAKE EXPERIMENTS

Diffusivity parameters were determined by fitting the model described by Equations (6)–(18) to differential uptake curves at pressures lower than

Table 4. Multisite Langmuir parameters for methane and nitrogen adsorption equilibrium on CMS 3K Takeda at 298, 308 and 323 K from 0–2000 kPa

Gas	$q_{max,i}$ [mol/kg]	K_i^o [1/kPa]	$-\Delta H_i$ [kJ/mol]	a_i [−]
CH_4	11.797	2.481×10^{-10}	38.947	6.303
N_2	10.623	6.567×10^{-7}	15.930	7.000

10 kPa. Fractional uptakes of methane, nitrogen and carbon dioxide at 298, 308, and 323 K are shown in Figs. 3 and 4, respectively. Note that in the case of methane, only experiments at one temperature (308 K) were reported.

Solid line in these figures corresponds to the fitting of the dual resistance model, which is good in all the cases. The parameters used to fit the curves (micropore diffusivity and the surface barrier mass transfer coefficient) are shown in Table 5.

The barrier mass transfer has a stronger effect in the initial part of the uptake. This effect is shown in Fig. 5 plotting the fractional uptake of methane and nitrogen at 308 K as a function of the square root of time (14, 17). The surface barrier in this adsorbent assumes an important role in the molecules with larger kinetic diameter, i.e., for methane the value is smaller than nitrogen.

The micropore diffusion of methane is very slow when compared to the other gases. This behavior was also reported in this kind of microporous adsorbents (8, 16, 35, 38). The order of magnitude of D_μ/r_μ^2 reported in all these works is comparable to the one obtained here but in this paper we are also including the surface barrier resistance. According to this dual-resistance model, the parameters are in agreement to the ones recently reported for Takeda adsorbents (17).

Diffusivity of nitrogen was also studied in literature (8, 13, 14, 16, 17, 33–35). In the case of CMS with pore mouth constriction, the surface barrier-micropore dual resistance model successfully represented the experimental data. From the uptake curves shown in this work, the dual-resistance model described by Eqs. (6)–(18) gives values in agreement with very recent ones reported for Takeda 3A molecular sieve carbon. In this work, the energy of activation of the micropore diffusivity is 34.7 kJ/mol, which compares very well with 35.2 and 32.9 kJ/mol reported by the group of prof. Farooq

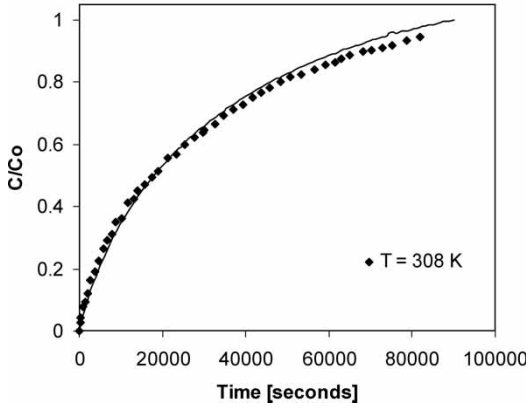

Figure 3. Fractional uptake of methane on Takeda CMS 3K at 308 K.; solid lines–dual resistance model.

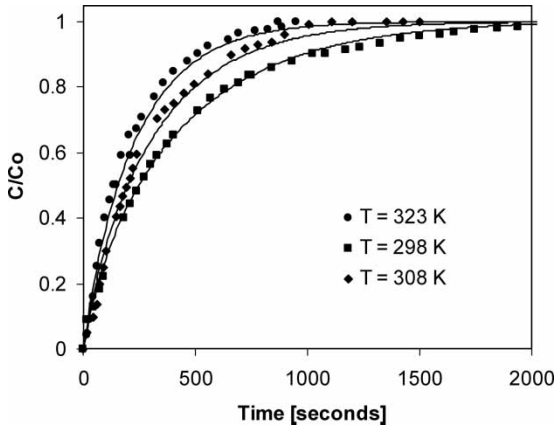

Figure 4. Fractional uptakes of nitrogen on Takeda CMS 3K. Symbols: ■ T = 298 K; ◆ T = 308 K; ● T = 323 K; solid lines–dual resistance model.

for Takeda 3A CMS (17); the energy of activation of the surface barrier is 5.87 kJ/mol, somewhat smaller than their reported value (28.7 kJ/mol).

The CMS 3K Takeda presented in this work presented higher equilibrium selectivity to methane (most adsorbed gas). Even though, as shown in Fig. 5, methane adsorbs very slowly and there is a large kinetic difference between the adsorption of these gases. Because of this difference in adsorption kinetics it is expected that this can be an appropriate adsorbent for methane–nitrogen splitting, adsorbing nitrogen and obtaining methane at high pressures without need of recompression, diminishing dramatically the costs of this separation when compared with cryogenic distillation.

FIXED-BED EXPERIMENTS

The final test of the adsorbent to perform the methane–nitrogen separation (and also the independent confirmation of the adsorption equilibrium and

Table 5. Kinetic parameters of the dual-resistance model for methane and nitrogen diffusion in CMS 3K at 298, 308, and 323 determined by batch adsorption uptake act low pressure

Gas	Temperature [K]	C_{B0} [mmol/l]	D_μ/r_μ^2 [s^{-1}]	k_b [s^{-1}]	$K_{\mu,i}$ [s^{-1}]
CH_4	308	4.38	2.33×10^{-6}	1.0×10^{-4}	2.59×10^{-5}
N_2	298	3.23	2.77×10^{-4}	6.0×10^{-3}	2.45×10^{-3}
	308	2.31	4.99×10^{-4}	6.4×10^{-3}	3.45×10^{-3}
	323	3.50	8.31×10^{-4}	7.2×10^{-3}	4.56×10^{-3}

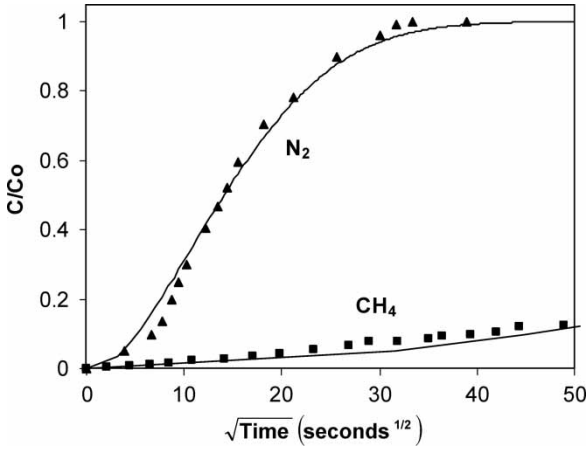

Figure 5. Fractional uptakes of methane and nitrogen at 308 K as a function of the square root of time. Symbols: ■ methane; ▲ nitrogen; solid lines–dual resistance model.

kinetic parameters determined by other techniques) is fixed-bed experiments. We have measured single component and binary breakthrough curves of the mixture nitrogen–methane. As explained before the adsorption kinetics was controlled by a dual contribution of micropore resistance and surface barrier resistance at the mouth of the micropore. In order to simplify this description to reduce computational time for PSA simulations, model equivalence was performed using the bi-LDF approach for bidisperse adsorbents. To confirm the applicability of the bi-LDF model to this system, pure component breakthrough curves with different molar fractions of adsorbates were performed. In all the cases, methane and nitrogen were diluted with helium considered as non-adsorbed gas. The LDF constants used for the simulation of all the results were calculated according to equations presented in Table 3 and are detailed in Table 5.

The curves using different molar fractions of methane (0.09, 0.43, 0.56 and 0.75) diluted in helium are presented in Fig. 6. The parameters used in the simulations (solid lines in the figure) are reported in Table 1. The data obtained for nitrogen diluted in helium (0.43, 0.53, 0.60, and 0.80) is also presented in Fig. 7. The solid lines in these plots represent the model described in Table 1 using the bi-LDF approach. It can be seen that using the bi-LDF simplification (instead of the complete model using micropore and surface barrier resistances) can describe well the single component breakthrough curves diluted in helium (assumed as nonadsorbed gas), at least in the experimental conditions and range of molar fractions covered by this study. In other studies dealing with adsorption of these gases in CMS 3A it was reported that the diffusivity coefficient, as well as the surface barrier resistance vary with adsorbed phase concentration (17, 37).

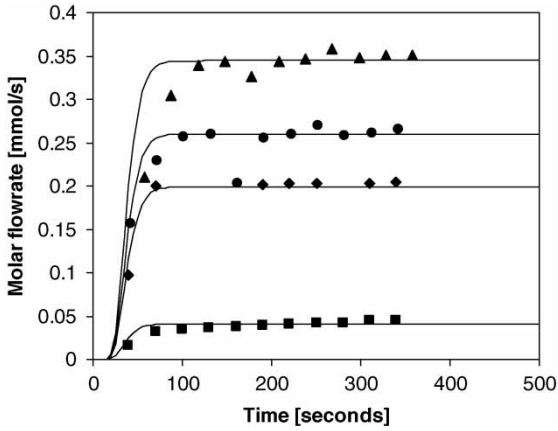

Figure 6. Breakthrough curves of methane (diluted in helium) in CMS 3K Takeda at ambient temperature and 250 kPa total pressure. Methane molar fractions: ■ 0.09; ◆ 0.43; ● 0.56; ▲ 0.75; solid lines are predictions with model shown in Table 3.

Data obtained for binary mixtures are presented in Fig. 8. Two different methane to nitrogen ratio were studied: 43/57 and 57/43. Temperature profiles measured in three different points of the column (0.18, 0.43, and 0.68 m from inlet) are also shown. The solid line in the plots are the model predictions using pure adsorption equilibrium and kinetic data (see Table 3) and shows good agreement with experiments, confirming that the data presented in this work can be used to model separation processes by

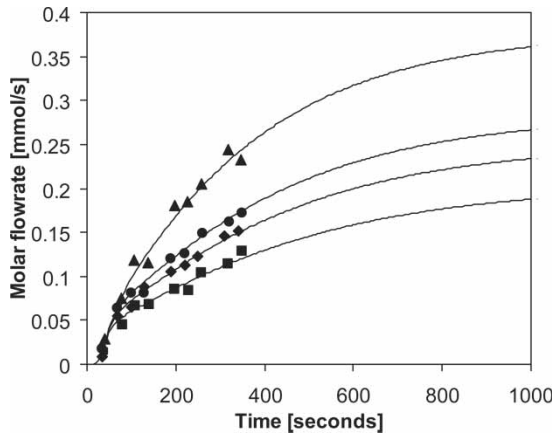

Figure 7. Breakthrough curves of nitrogen (diluted in helium) in CMS 3K Takeda at ambient temperature and 250 kPa total pressure. Methane molar fractions: ■ 0.43; ◆ 0.53; ● 0.60; ▲ 0.80; solid lines are predictions with model shown in Table 3.

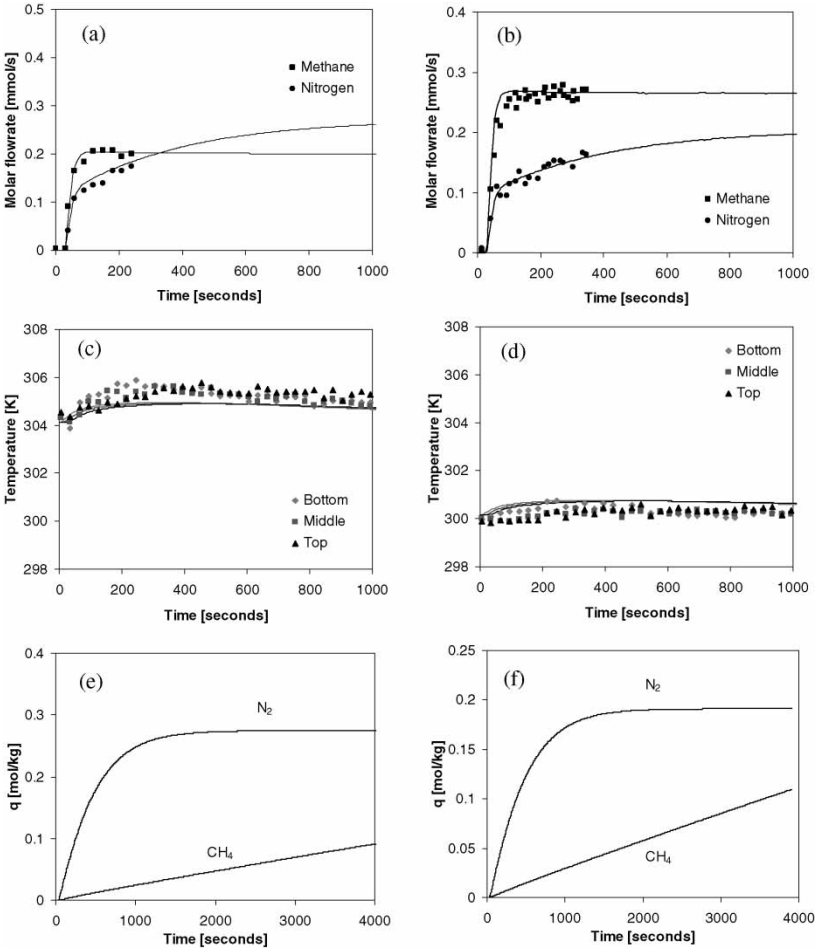

Figure 8. Breakthrough curves of methane–nitrogen mixtures at 250 kPa total pressure and ambient temperature. (a, b) molar flow exiting the column; (c, d) temperature profiles measured at 0.18, 0.43, and 0.68 m from feed inlet and (e, f) simulated amount adsorbed evolution of particles at the end of the column. Figures a, c, and e correspond to mixture 0.43–0.57 (methane–nitrogen) while b, d, and f —correspond to mixture 0.57–0.43 (methane–nitrogen).

adsorption. As observed with the pure gas breakthrough experiments, the data obtained here confirms the nearly isothermal behavior of the system, with a very small temperature increase due to release of heat of adsorption. In Fig. 8 the simulation of the evolution of the amount adsorbed in the particles at the length of the column is also shown. Even when the outlet concentration seems to remain constant it can be seen that the adsorbent is still adsorbing methane, which is far away from the adsorption equilibrium.

These results showed by the binary breakthrough curves can be understood defining a kinetic selectivity factor, relating the adsorbed phase concentration and the kinetics of diffusion of each component (6):

$$\beta_{SEL} = \frac{q_{N_2}}{q_{CH_4}} \sqrt{\frac{K_{\mu,N_2}}{K_{\mu,CH_4}}} \tag{22}$$

Evaluating this factor at 308 K for the methane to nitrogen ratio 57/43, the square root gives a factor of 11.5 favorable to nitrogen adsorption. The difference in the kinetics of adsorption of the two gases to separate is even larger than for nitrogen purification from air (18). Despite of this difference in diffusion constants, the ratio of amount adsorbed is 0.165 (much more methane adsorbed than nitrogen when equilibrium is established), resulting in an overall kinetic selectivity of 1.9.

No other binary breakthrough experiments were found in literature. Some PSA experiments using Bergbau-Forschung CMS adsorbent also showed low selectivity of carbon molecular sieves for methane purification from nitrogen-contaminated streams (39). Even when the selectivity of this adsorbent is low, it is interesting to investigate its performance in the separation of methane – nitrogen because of unnecessary product recompression, being an interesting economic alternative to small and medium natural gas drills or landfill gas methane recovery.

CONCLUSIONS

Adsorption equilibrium measured in a gravimetric device for methane and nitrogen are reported at 298, 308, and 323 K on CMS 3K Takeda at pressures up to 2000 kPa. The data were fitted with the multisite Langmuir model. Methane is more adsorbed than nitrogen in this adsorbent. Even though, the diffusion of methane is very slow taking three days to achieve one equilibrium point.

It was observed that for both gases, a surface barrier resistance at the mouth of the micropores and the micropore resistance share the control of the diffusion process: at 308 K, $D_\mu/r_\mu(CH_4) = 2.33\ \ 10^{-6}\,s^{-1}$ and $k_b(CH_4) = 1.0\ \ 10^{-4}\,s^{-1}$ and $D_\mu/r_\mu(N_2) = 4.99\ \ 10^{-4}\,s^{-1}$ and $k_b(N_2) = 6.4\ \ 10^{-3}\,s^{-1}$. These values indicate a large difference in adsorption kinetics appropriate to adsorb nitrogen and reject methane.

Single component breakthrough curves were performed at ambient temperature to confirm the validity of using the bi-LDF approach instead of the complete model (considering macropore, micropore and surface barrier resistance). Binary methane–nitrogen breakthrough curves were also performed to determine the behavior of the adsorbent for the separation of the mixture. The difference in the kinetics of adsorption of methane and nitrogen is very large, but the amount of nitrogen adsorbed is much smaller than methane, resulting

in a small overall kinetic selectivity. At 308 K for the mixture 57-43 (methane to nitrogen ratio) the kinetic selectivity was 1.9.

Even when the selectivity of this adsorbent is low, it is interesting to investigate its performance in the separation of methane–nitrogen because of unnecessary product recompression, being an interesting economic alternative for natural gas or landfill gas methane recovery. The data reported in this work can be used for modeling adsorption based separation processes, like Pressure Swing Adsorption, for natural or landfill methane upgrade.

NOMENCLATURE

a'	area to volume ratio (m^{-1})
a_i	number of neighboring sites occupied by component i
Bi	Biot number
C_i	gas concentration in the fluid phase for component i (mol/m^3)
$\langle c_i \rangle$	averaged concentration in the macropores for component i (mol/m^3)
C_B	bulk gas concentration (mol/m^3)
C_{Bo}	initial gas concentration (mol/m^3)
$\tilde{C}_p$	molar constant pressure specific heat of the gas mixture ($J/mol \cdot K$)
$\tilde{C}_{ps}$	constant pressure specific heat of the adsorbent ($J/kg \cdot K$)
$\hat{C}_{pw}$	specific heat of the column wall ($J/kg \cdot K$)
C_T	total gas concentration (mol/m^3)
$\tilde{C}_v$	molar constant volumetric specific heat of the gas mixture, ($J/mol \cdot K$)
$\tilde{C}_{v,\text{ads}}$	molar constant volumetric specific heat of the gas mixture adsorbed ($J/mol \cdot K$)
d_p	pellet diameter (m)
$D_{ax,i}$	axial dispersion coefficient of component i (m^2/s)
D_{AA}	self-diffusivity (m^2/s)
$D_{\mu,i}$	micropore diffusivity of component i (m^2/s)
$D_{k,i}$	Knudsen diffusion of component i (m^2/s)
$D_{p,i}$	pore diffusivity of component i (m^2/s)
$k_{b,i}$	barrier mass transfer coefficient for component i (s^{-1})
k_f	external mass transfer resistance (m/s)
K_i	equilibrium constant of component i (1/kPa)
K_i^0	exponential parameter of the equilibrium constant for component i (1/kPa)
$K_{P,i}$	Linear Driving Force constant for macropore diffusion of component i (s^{-1})
$K_{\mu,i}$	Linear Driving Force constant for micropore diffusion (micropore + surface barrier) of component i (s^{-1})

h_f	film heat transfer coefficient between the gas and the solid phase ($W/m^2 \cdot K$)
h_w	film heat transfer coefficient between the gas phase and the column wall ($W/m^2 \cdot K$)
m_{ads}	adsorbed mass (kg)
m_s	mass of adsorbent connected to the microbalance (kg)
M_W	molecular weight of gas (g/mol)
P	pressure (kPa)
P_c	critical pressure (atm)
q_i	absolute adsorbed phase concentration of component i (mol/kg)
q_{exc}	excess adsorbed phase concentration (mol/kg)
$q_{max,i}$	maximum adsorbed phase concentration (mol/kg)
q_i^*	equilibrium adsorbed phase concentration (mol/kg)
$\overline{q}_i$	crystal-averaged adsorbed phase concentration of component i (mol/kg)
$\langle \overline{q_i} \rangle$	extrudate-averaged adsorbed phase concentration of component i (mol/kg)
r	distance along microparticles radius (m)
r_μ	radius of the microparticles (m)
r_p	pore radius (m)
R	distance along macroparticles radius (m)
R_g	ideal gas constant, 8.314 ($J/mol \cdot K$)
R_p	radius of extrudate (m)
R_w	column internal radius (m)
T	temperature (K)
T_c	critical temperature (K)
T_g	temperature of the gas-phase (K)
T_s	solid (extrudate) temperature) (K)
T_w	wall temperature (K)
T_∞	column surrounding temperature (K)
u	superficial velocity (m/s)
U	global external heat transfer coefficient ($W/m^2 \cdot K$)
V	volume of the adsorbent and adsorbate (m^3)
V_{ads}	volume of the adsorbed phase (m^3)
V_s	volume of adsorbent obtained by calibration with helium (m^3)
V_c	microbalance cell volume obtained by calibration with helium (m^3)
y_i	molar fraction of component i in the gas phase

Greek Letters

ε_c	column void fraction
ε_p	porosity of the pellet

ρ_b	density in the bulk (kg/m^3)
ρ_G	gas density (kg/m^3)
ρ_L	liquid density of the gas in a reference state (kg/m^3)
ρ_p	density of the pellet (kg/m^3)
ρ_w	density of the wall (kg/m^3)
α_k	kinetic separation factor
α_w	ratio of the internal surface area to the volume of the column wall (m^{-1})
α_{wl}	ratio of the logarithmic mean surface area of the column shell to the volume of the column wall (m^{-1})
τ_p	tortuosity of the pellet
$-\Delta H_i$	isosteric heat of adsorption of component i (multisite Langmuir model) (kJ/mol)
Δm	microbalance signal (mg)
μ_g	gas viscosity (Pa.s)

ACKNOWLEDGMENT

The authors would like to thank financial support from Foundation for Science and Technology (FCT) by project POCTI/1999/EQU/32654 and grants: SFRH/BD/1457/2000 and SFRH/BD/11398/2002.

REFERENCES

1. Cummins Westport Inc. homepage: http://www.cumminswestport.com/fuels/index.php (Accessed Nov 2004).
2. *Ullmann's Encyclopedia of Industrial Chemistry*, 7th Edition., Wiley-VCH, Verlag GmbH & Co.KGaA, 2003.
3. Knaebel, K.S. and Reinhold, H.E. (2003) Landfill gas: From rubbish to resource. *Adsorption*, 9: 87–94.
4. Kapoor, A. and Yang, R.T. (1989) Kinetic separation of methane/carbon dioxide by adsorption on molecular sieve carbon. *Chem. Eng. Sci.*, 44: 1723–1733.
5. US EPA Doc 430-R-97-012. Technical and Economic Assessment of Potential to Upgrade Gob Gas to Pipeline Quality. Dec. 1997. (www.epa.gov, accessed in Nov 2004).
6. Habgood, H.W. (1958) The kinetics of molecular sieve action. Sorption of nitrogen–methane mixtures by linde molecular sieve 4A. *Can. J. Chem.*, 36: 1384–1397.
7. Chihara, K., Suziki, M., and Kawazoe, K. (1978) Adsorption rate on molecular sieving carbon by chromatography. *AIChE J*, 24: 237–246.
8. Ma, Y.H., Sun, W., Bhandarkar, M., Wang, J., and Miller, G.W. (1991) Adsorption and diffusion of nitrogen, oxygen, argon, and methane in molecular sieve carbon at elevated pressures. *Separations Technology*, 1: 90–98.
9. Vyas, S.N., Patwardhan, S.R., Vijayalakshmi, S., and Sri Ganesh, K. (1994) Adsorption of gases on carbon molecular sieves. *J. Col. Interf. Sci.*, 168: 275–280.

10. Yang, R.T. (2003) *Adsorbents. Fundamentals and Applications*; J. Wiley: New Jersey.
11. Engelhard Corporation. *Purification Technologies Brochure*; 2001.
12. Jüntgen, H., Knoblauch, K., and Harder, K. (1981) Carbon molecular sieves: Production from coal and applications in gas separation. *Fuel*, 60: 817–822.
13. Ruthven, D.M., Raghavan, N.S., and Hassan, M.M. (1986) Adsorption and diffusion of nitrogen and oxygen in a carbon molecular sieve. *Chem. Eng. Sci.*, 41: 1325–1332.
14. Srinivasan, R., Auvil, S.R., and Schork, J.M. (1995) Mass transfer in carbon molecular sieves–an interpretation of Langmuir kinetics. *The Chem. Eng. J.*, 57: 137–144.
15. Shen, D., Bülow, M., and Lemcoff, N. (2003) Mechanisms of molecular mobility of oxygen and nitrogen in carbon molecular sieves. *Adsorption*, 9: 295–302.
16. Jayaraman, A., Chiao, A.S., Padin, J., Yang, R.T., and Munson, C.L. (2002) Kinetic separation of methane/carbon dioxide by molecular sieve carbons. *Sep. Sci. and Tech.*, 37: 2505–2528.
17. Qinglin, H., Sundaram, S.M., and Farooq, S. (2003) Revisiting transport of gases in the micropores of carbon molecular sieves. *Langmuir*, 19: 393–405.
18. Schröter, H.J. and Jüntgen, H. (1988) Gas separation by pressure swing adsorption using carbon molecular sieves. In *Adsorption: Science and Technology*; Rodrigues, LeVan and Tondeur, eds.; NATO ASI Series, Kluwer Academic Publishers: Netherlands.
19. Da Silva, F.A. (1999) Cyclic adsorption processes: Application to propane/propylene separation. Ph.D. Dissertation, University of Porto, Portugal.
20. Murata, K., Miyawaki, J., and Kaneko, K. (2002) A simple determination method of the absolute adsorbed amount for high pressure gas adsorption. *Carbon*, 40: 425–428.
21. Murata, K. and Kaneko, K. (2000) Nano-range interfacial layer upon high-pressure adsorption of supercritical gases. *Chem. Phys. Letters*, 321: 342–348.
22. Dreisbach, F., Staudt, R., and Keller, J.U. (1999) High pressure adsorption data of methane, nitrogen, carbon dioxide and their binary and ternary mixtures on activated carbon. *Adsorption*, 5: 215–227.
23. Ustinov, E.A., Do, D.D., Herbst, A., Staudt, R., and Harting, P. (2002) Modeling of gas adsorption equilibrium over a wide range of pressure. A thermodynamic approach based on equation of state. *J. Col. Interf. Sci.*, 250: 49–62.
24. Cavenati, S., Grande, C.A., and Rodrigues, A.E. (2004) Adsorption equilibrium of methane, carbon dioxide and nitrogen on zeolite 13X at high pressures. *J. Chem. Eng. Data*, 49: 1095–1101.
25. Nitta, T., Shigetomi, T., Kuro-Oka, M., and Katayama, T. (1984) An adsorption isotherm of multi-site occupancy model for homogeneous surface. *J. Chem. Eng. Japan.*, 17: 39–45.
26. Farooq, S., Qinglin, H., and Karimi, I.A. (2002) Identification of transport mechanism in adsorbent micropores from column dynamics. *Ind. Eng. Chem. Res.*, 41: 1098–1106.
27. Loughlin, K.F., Hassan, M.M., Fatehi, A.I., and Zahur, M. (1993) Rate and equilibrium sorption parameters for nitrogen and methane on carbon molecular sieve. *Gas Sep. Pur.*, 7: 264–273.
28. Chagger, H.K., Ndaji, F.E., Sykes, M.L., and Thomas, K.M. (1995) Kinetics of adsorption and diffusional characteristics of carbon molecular sieves. *Carbon*, 33 (10): 1405–1411.

29. Sircar, S. (2001) Measurement of gibbsian surface excess. *AIChE J*, 47: 1169–1176.
30. Bird, R.B., Stewart, W.E., and Lightfoot, E.N. (2002) *Transport Phenomena*. 2nd ed.; Wiley International: Singapore.
31. Grande, C.A. and Rodrigues, A.E. (2004) Adsorption of binary mixtures of propane–propylene in carbon molecular sieve 4A. *Ind. Eng. Chem. Res.*, 43: 8057–8065.
32. Chen, Y.D. and Yang, R.T. (1994) Preparation of carbon molecular sieve membrane and diffusion of binary mixtures in the membrane. *Ind. Eng. Chem. Res.*, 33: 3146–3153.
33. Schalles, D.G. and Danner, R.P. (1988) Adsorption of oxygen and nitrogen on carbon molecular sieve type 3A. In: Adsorption and Ion Exchange. *AIChE Symposium Series*, 84 (264): 83–88.
34. Reid, C.R. and Thomas, K.M. (1999) Adsorption of gases on a carbon molecular sieve used for air separation: Linear adsorptives as probes for kinetic selectivity. *Langmuir*, 15: 3206–3218.
35. Ackley, M.W. and Yang, R.T. (1990) Kinetic separation by pressure swing adsorption: Method of characteristics model. *American Institute of Chemical Engineers Journal*, 36: 1229–1238.
36. Rutherford, S.W. and Coons, J.E. (2003) Adsorption dynamics of carbon dioxide in molecular sieving carbon. *Carbon*, 41: 405–411.
37. Rutherford, S.W., Nguyen, J.E., Coons, J.E., and Do, D.D. (2003) Characterization of carbon molecular sieves using methane and carbon dioxide as adsorptive probes. *Langmuir*, 19: 8335–8342.
38. Bae, Y.S. and Lee, C.H. (2005) Sorption kinetics of eight gases on a carbon molecular sieve at elevated pressures. *Carbon*, 43: 95–107.
39. Fatehi, A.I., Loughlin, K.F., and Hassan, M.M. (1995) Separation of methane–nitrogen mixtures using a carbon molecular sieve. *Gas Sep. Pur.*, 9: 199–204.